Multibeam Stimulated Brillouin Scattering from Hot Solid-Target Plasmas

Introduction

We report on the first multibeam laser–plasma interaction experiments with a critical density surface present at all times. Six interaction beams are incident on a preformed plasma, tailored to resemble future direct-drive-ignition laser fusion implosions. Stimulated Brillouin scattering (SBS) was observed using two full-aperture backscattering stations. The results show strong evidence of electromagnetic (EM) wave seeding of SBS backscatter and may also indicate strongly driven, common, symmetrically located ion waves. The latter could provide for efficient sidescattering that provides the EM seed for SBS backscattering. Quenching SBS before the peak of the interaction beam is seen in all the experiments. For NIF direct-drive ignition experiments the expected SBS levels are well below 1%.

The details of laser coupling to the hot coronal plasma of direct-drive inertial confinement fusion (ICF) targets are extremely important since the laser provides the drive energy for the implosion.[1] Measurement and understanding of power (or energy) loss due to SBS are essential. Over the past 30 years, many detailed reports[2–12] of SBS experiments have been published; however, few, if any, have investigated conditions relevant to direct-drive ICF plasma implosions.[4] In direct-drive implosions, many individual laser beams are overlapped on the target. This allows multibeam interactions that may change the SBS instability characteristics.[13,14] In particular, SBS instability can grow from an EM wave seed provided by other beams reflected near the critical-density surface, or common (shared) ion waves can reduce the instability threshold. Previous multibeam SBS experiments[3,15] have been performed in plasmas with peak densities significantly lower than critical density and are, thus, not directly applicable to direct-drive ICF conditions. Those experiments indicated a redistribution of the scattered light but no significant increase in the overall SBS losses.[15]

In future direct-drive-ignition experiments on the National Ignition Facility (NIF),[16] the conditions most vulnerable to SBS will occur before the laser reaches its peak power[1] and will correspond to plasmas with $T_e \gtrsim 2$ keV and density and velocity scale lengths of ~0.5 mm. These will be irradiated with 351-nm laser light with laser-beam smoothing[17] by spectral dispersion (SSD) at ~1 THz and polarization smoothing (PS). The corresponding single-beam irradiation intensities are $\lesssim 10^{14}$ W/cm^2 (four beamlets, or one quad, of the NIF[16]).

The full plasma and intensity evolution of a NIF direct-drive implosion cannot be simulated with present laser systems, but a good approximation to the conditions that are most susceptible to SBS can be achieved using OMEGA. Past single-beam interaction experiments on OMEGA have shown that SBS is unlikely to represent a significant energy loss during the high-intensity portion of the NIF pulse.[4] The present multiple-beam SBS experiments are the first reported in the literature with a critical-density surface present at all times and plasma conditions close to those expected on the NIF. Six interaction beams are symmetrically arrayed around the target normal. These interaction beams are overlapped on a plasma produced from a thick CH target by heater beams that strike the target in advance of the interaction beams.

Experiments

The experiments were carried out on the OMEGA laser system[18] using a subset of its 60 UV (351-nm) beams. The experimental arrangement is shown schematically in Fig. 87.21. The CH targets were 100 μm thick and 5 mm in diameter (semi-infinite) with their normal pointed toward the center of the six symmetrically arranged interaction beams (see Figs. 87.21 and 87.22). These targets were sequentially irradiated with nine primary beams, followed in 1-ns intervals by six secondary heater beams and six interaction beams. The six interaction beams are identified with their beam numbers inside the circles in Fig. 87.22 and are located at ~ 23° to the target normal. The primary and secondary beams are at ~62° and 48° to the target normal, respectively.

All of the beams were equipped with distributed phase plates[19] (DPP's) and were operated with 2-D SSD (1 THz) and PS.[17] The phase plates in the primary and secondary beams

were standard OMEGA "SG3" phase plates (nominally Gaussian spots of 0.5-mm FWHM at best focus). These beams were defocused to produce a 2-mm-diam spot (~1-mm FWHM) with peak intensities (averaged over the speckle pattern) of $\sim 4 \times 10^{13}$ W/cm^2. Two alternative configurations were used on the six interaction beams: All were outfitted with either six standard phase plates with the target at best focus (nominal single-beam peak intensity of 2×10^{14} W/cm^2) or three pairs of phase plates that produced smaller spots. In the latter case, the corresponding average single-beam peak intensities were 4, 8, and 16×10^{14} W/cm^2. The beam energy for all shots was ~365 J (±5%). The laser pulse shapes were a close approximation of those shown schematically in Fig. 87.21, i.e., a 0.5-ns linear rise followed by a 0.9-ns flattop.

Similar preformed plasmas have been diagnosed extensively using time-resolved x-ray spectroscopy, time-resolved stimulated Raman scattering (SRS) spectroscopy,[4] and schlieren photography.[5,20] Those experiments have been simulated with the two-dimensional hydrodynamic code *SAGE*.[21] Because the *SAGE* simulations have generally closely replicated the measurements, we are confident that the *SAGE* predictions for the present experiments are equally valid: electron temperatures of ~2 to 3 keV with electron density and velocity scale lengths of ~1 mm.

Two full-aperture backscatter (FABS) stations were used to measure the SBS energies and the time-resolved SBS spectra. These stations collected the light propagated from the target in the direction opposite to the incoming high-energy beam path through the *f*/6 OMEGA focusing lens. This was accomplished using an uncoated, wedged, fused quartz optic ahead of the focusing lens. The arrangement allows the incoming high-energy beam to pass onward to the target while a full-aperture, reduced-energy sample of any outbound light is delivered to the FABS setup. Beams 25 and 30 (in Fig. 87.22) were instrumented in this manner. Within the FABS, the energies were measured with appropriately filtered and cross-calibrated calorimeters. The light for the time-resolved spectra was focused through an engineered diffuser (2° scattering angle)

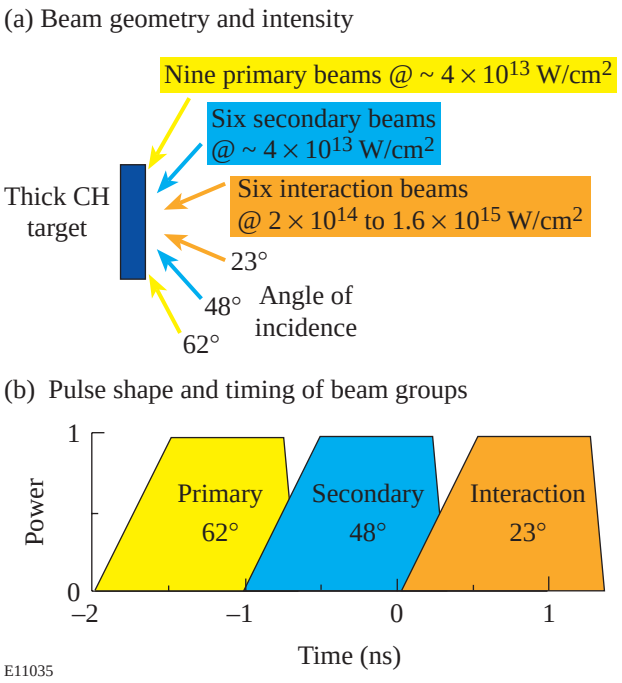

Figure 87.21
Schematic representation of solid-target illumination with three sets of laser beams. Pulse sequence, pulse shapes, and approximate angles of incidence are indicated. The irradiation intensity of each primary and secondary beam is ~4×10^{13} W/cm^2; the interaction-beam intensities vary from 2×10^{14} to 1.6×10^{15} W/cm^2.

Beam number	25	30	12	23	14	50
I_{14} (10^{14} W/cm^2)	4	16	4	8	16	8

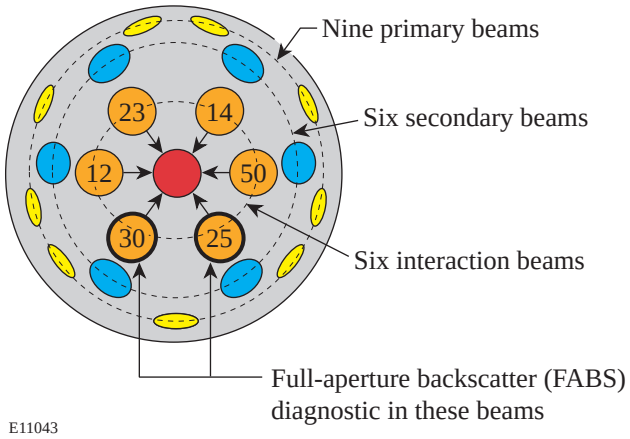

Figure 87.22
Schematic representation of the plasma-producing and interaction beams on the target chamber surface. The numbers inside the circles are the beam numbers for the interaction beams. Beams 25 and 30 are outfitted with full-aperture backscatter (FABS) stations. All beam energies are nominally 365 J. The intensities (in units of 10^{14} W/cm^2) shown in the boxes below the beam numbers result from three different sets of phase plates. Standard OMEGA phase plates also permitted interaction intensities of 2×10^{14} W/cm^2 in any or all of the beams.

into 435-μm gradient-index fibers and sent to a 1-m grating spectrometer coupled to an S20 streak camera. The fibers from both FABS stations were time-multiplexed at the input to the spectrometer. The measured time resolution was 80 ps and the dynamic spectral resolution was ~0.4 Å.

Results

The multibeam, time-integrated SBS reflectivity is shown in Fig. 87.23 as a function of the interaction beam intensity. Data from both FABS stations are shown. The average peak intensities of the various interaction beams ranged from 2×10^{14} W/cm^2 to 1.6×10^{15} W/cm^2, depending on the phase plates used. The average peak intensity I_{95} is defined such that 95% of the laser energy has intensities at or below I_{95}. Thus, most shots yielded simultaneous multibeam backscatter data at two intensities. The squares in Fig. 87.23 represent through-the-lens reflectivities with all beams at nominal energy. The diamonds represent shots without interaction beams (e.g., without beam 25 for FABS25), while the circles represent shots without the beams opposing the interaction beams [beam 23 for FABS25, beam 14 for FABS30 (see Fig. 87.22)].

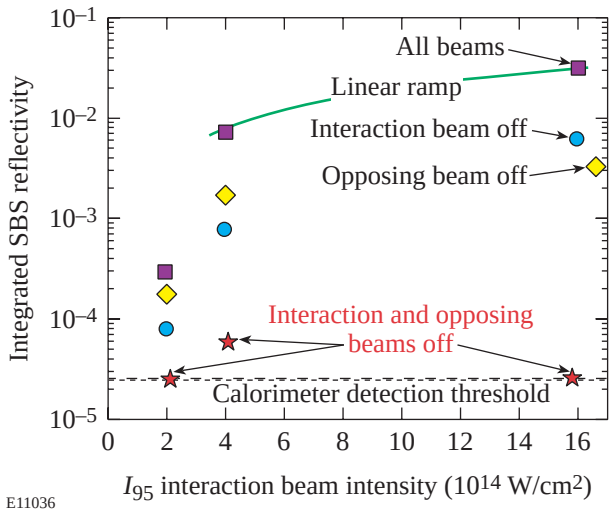

Figure 87.23
Multibeam, time-integrated SBS reflectivity measured by the calorimeters in two different locations (FABS25 and FABS30) for beam smoothing with 1-THz, 2-D SSD and PS. Squares represent measurements with all beams as indicated in Fig. 87.22, diamonds indicate shots without interaction beams (either beam 25 for FABS25 or beam 30 for FABS30), circles indicate shots without beams opposing the interaction beams (beam 23 for FABS25, beam 14 for FABS30). The stars indicate FABS energy measurements normalized to the mean beam energy with beams 25 and 23 (or 30 and 14) turned off. The linear ramp is shown to guide the eye and is indicative of saturation at intensities in excess of ~3×10^{14} W/cm^2. Each point plotted represents several actual shots with the shots clustered within the symbols shown.

The possible interplay and synergistic enhancement between specular reflection at the turning point, SBS sidescattering, and SBS backscattering are depicted in Fig. 87.24. Given the geometry of the interaction beams, the "opposing" beams (e.g., 23 and 14) are reflected at their respective turning points near the critical density ($n_e \sim 0.88\ n_c$) and counterpropagate into beams 25 and 30. (Note: In this discussion, the term "opposing beam" means the beam on the opposite side of the circle of interaction beams. This is not the beam on the opposite side of the OMEGA target chamber that has a coincident optical axis, which was not used in these experiments.) These reflections can provide EM seed waves for SBS backscattering in beams 25 and 30. This is reminiscent of external EM-wave-seeding experiments by Baldis[3] and Fernandez.[6] In addition, the specular reflections can also provide EM seeds for SBS sidescattering in that direction.

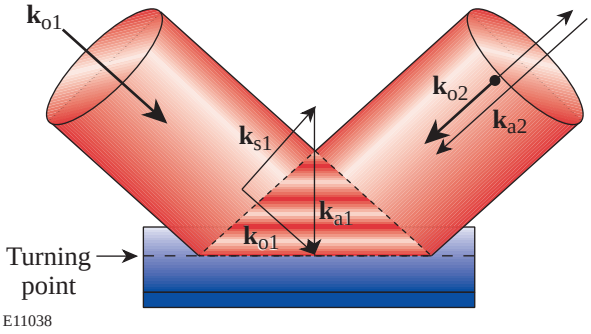

Figure 87.24
Schematic visualization of the interplay between SBS sidescattering and SBS backscattering on flat targets irradiated with symmetrically positioned interaction beams. The specular reflection at the turning point provides an EM seed for SBS sidescattering. That, in turn, provides an efficient EM seed for SBS backscattering of the "opposing" beam. These processes are most effective near the sonic point where the SBS wavelength shifts vanish.

The overall, multibeam reflectivities (squares in Fig. 87.23) saturate at a few percent for average irradiation intensities of 3 to 4×10^{14} W/cm^2. Selectively turning off one of the interaction beams (beam 25 or 30—circles) or one of their opposing beams (beam 23 or 14—diamonds) leads to a significant drop in reflectivity. Furthermore, if both the interaction beam and its opposing beam are turned off, the residual reflectivities (stars) drop to the detection threshold for all but the point at 4×10^{14} W/cm^2. For this point, the high-intensity beams 30 and 14 cause measurable sidescatter signal. For the other two intensities, the four remaining beams are too low in intensity to produce measurable SBS sidescattering into either

FABS25 or FABS30. Pure SBS backscattering for oblique incidence (circles) is observed if the beam opposing the interaction beam (e.g., beam 23) is turned off. In this case SBS grows from either noise or any existing seed (e.g., stars in Fig. 87.23).

The measured reflectivity in FABS25 is roughly twice that measured for pure backscattering when beam 25 is removed while the opposing beam 23 is left on. This signal (diamonds) represents SBS sidescattering of beam 23, which may be enhanced through ion-wave seeding by the symmetrically located ion waves produced by cooperative multibeam SBS side scattering from the other four interaction beams (see Fig. 87.24). In addition, this sidescatter SBS may also be EM-seeded by its own reflection at the turning point. As a result, the two processes cannot be separated by this measurement alone. As will be discussed later, both the sidescattering and backscattering power reflectivities peak before the maximum of the laser pulse and have essentially identical power histories.

When all beams are turned on (squares in Fig. 87.23), the signal is much stronger than a linear superposition of the backscatter and sidescatter signals. The backscatter signal by itself (circles) is negligible, while the sidescatter signal (diamonds) provides the main EM seed for backscattering when all beams are turned on.

Representative time-resolved power reflectivities are shown in Fig. 87.25 for two experimental conditions. The power reflectivities at other intensities as well as the sidescatter power reflectivities (corresponding to the diamonds in Fig. 87.23) show similar temporal behaviors: they peak well before the laser pulse reaches its maximum. This rules out a linear scattering (or reflection or refraction) process that would peak toward the end of the laser pulse due to the heating of the plasma by the interaction beams. These power reflectivities show that the SBS backscatter and sidescatter signals are quenched before the peak of the laser pulse, possibly due to filamentation. A similar suppression of SBS forward scattering due to filamentation has been observed recently in experiments by Fuchs *et al.*[11] and in simulations by Tikhonchuk.[10,12]

The measured multibeam reflectivities in FABS25 (squares in Fig. 87.23) are principally EM-seeded backscattering of beam 25 with the seed provided by SBS sidescattering of the opposing beam 23. The ion waves involved in this process are the same as those involved in the cooperative multibeam SBS process of beams 14 and 30, 12 and 52 (see Fig. 87.22). To check whether these common ion waves indeed play a role in the sidescattering of beam 23, the intensities of several of the four beams were varied; the resulting FABS25 reflectivities are shown in Fig. 87.26 as a function of overlapped intensity. The sidescatter reflectivity declined with decreasing overlapped intensity of the four beams while the energies and intensities in beams 25 and 23 were kept constant. Thus, the differences in measured FABS25 reflectivities are clearly associated with the four asymmetrically located interaction beams. These same beams provide only a negligible EM seed to the SBS backscatter signal in FABS25 (stars in Fig. 87.23), but they do heat the plasma. These observations are consistent with the existence of common, symmetrically located ion waves produced by these four beams; these ion waves contribute significantly to the sidescattering of beam 23 into beam 25. Since the SBS reflectivities in Fig. 86.26 are well into the saturated regime, we estimate that the ion-wave amplitudes decline roughly by the same factor as the reflectivities. Alternatively, the change in electron temperature with increasing overlapped irradiation intensity may increase the EM seed for sidescattering, and consequently, also the total seed provided for backscattering. In this case no common ion waves would be involved. Our present experiments cannot rule out this scenario.

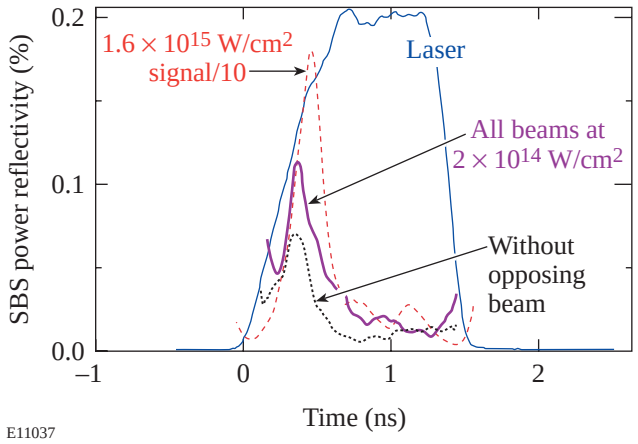

Figure 87.25
Measured multibeam SBS reflectivities for three different irradiation conditions along with a typical laser pulse shape. The dashed line is the backscatter signal in FABS30 for the irradiation conditions shown in Fig. 87.22. The dotted line and the thick solid line represent backscattering at low irradiation intensities with all interaction beams at 2×10^{14} W/cm^2. For the dotted line the opposing beam 23 was turned off, resulting in pure backscattering of beam 25.

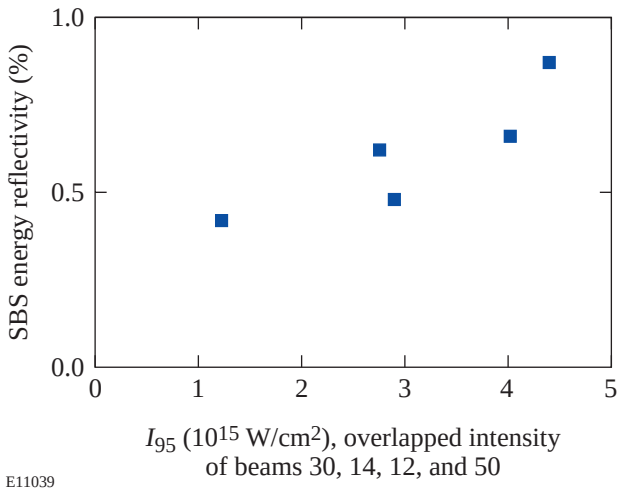

Figure 87.26
Backscatter reflectivities measured with FABS25 for the general irradiation conditions shown in Fig. 87.22 with some variations in beam energies of beams 30 and 14. The beam energies in beams 25 and 23 were kept constant. The increase in reflectivity with increasing overlapped intensity may be associated with a change in the common ion-acoustic-wave amplitudes generated by beams 30, 14, 12, and 50. Alternatively, the increase may be a consequence of decreased absorption as the plasma temperature increases with increasing overlapped intensity on target.

Conclusions

Multibeam interaction experiments were carried out in NIF-type, hot, long-scale-length plasmas on OMEGA using thick, planar CH targets. A symmetrical arrangement of six interaction beams with beam smoothing is consistent with strongly driven common ion waves located along the axis of symmetry of the six interaction beams. The present experiments, however, cannot rule out alternative interpretations that do not involve common ion waves. In either case, SBS sidescattering provides a large EM seed for SBS backscattering. These experiments have shown for the first time the synergistic enhancement of SBS sidescattering and backscattering. The fact that backscatter levels well below 1% are expected for typical NIF direct-drive irradiation conditions provides confidence in the expected direct-drive target performance on the NIF.[22]

ACKNOWLEDGMENT

This work was supported by the U.S. Department of Energy Office of Inertial Confinement Fusion under Cooperative Agreement No. DE-FC03-92SF19460, the University of Rochester, and the New York State Energy Research and Development Authority. The support of DOE does not constitute an endorsement by DOE of the views expressed in this article.

REFERENCES

1. S. E. Bodner, D. G. Colombant, J. H. Gardner, R. H. Lehmberg, S. P. Obenschain, L. Phillips, A. J. Schmitt, J. D. Sethian, R. L. McCrory, W. Seka, C. P. Verdon, J. P. Knauer, B. B. Afeyan, and H. T. Powell, Phys. Plasmas **5**, 1901 (1998).
2. C. J. Walsh, D. M. Villeneuve, and H. A. Baldis, Phys. Rev. Lett. **53**, 1445 (1984).
3. D. M. Villeneuve, H. A. Baldis, and J. E. Bernard, Phys. Rev. Lett. **59**, 1585 (1987).
4. S. P. Regan, D. K. Bradley, A. V. Chirokikh, R. S. Craxton, D. D. Meyerhofer, W. Seka, R. W. Short, A. Simon, R. P. J. Town, B. Yaakobi, J. J. Caroll III, and R. P. Drake, Phys. Plasmas **6**, 2072 (1999).
5. W. Seka, R. E. Bahr, R. W. Short, A. Simon, R. S. Craxton, D. S. Montgomery, and A. E. Rubenchik, Phys. Fluids B **4**, 2232 (1992).
6. J. C. Fernández *et al.*, Phys. Rev. Lett. **81**, 2252 (1998).
7. J. C. Fernández *et al.*, Phys. Plasmas **4**, 1849 (1997).
8. J. A. Cobble *et al.*, Phys. Plasmas **7**, 323 (2000).
9. C. Labaune *et al.*, Phys. Rev. Lett. **85**, 1658 (2000).
10. V. T. Tikhonchuk *et al.*, Phys. Plasmas **8**, 1636 (2001).
11. J. Fuchs *et al.*, Phys. Plasmas **7**, 4659 (2000).
12. J. Myatt *et al.*, "Nonlinear Propagation of a Randomized Laser Beam Through an Expanding Plasma," to be published in Physical Review Letters.
13. D. F. DuBois, B. Bezzeridels, and H. A. Rose, Phys. Fluids B **4**, 241 (1992).
14. H. A. Rose and D. F. DuBois, Phys. Fluids B **4**, 252 (1992).
15. H. A. Baldis *et al.*, Phys. Rev. Lett. **77**, 2957 (1996).
16. J. D. Lindl, *Inertial Confinement Fusion: The Quest for Ignition and Energy Gain Using Indirect Drive* (Springer-Verlag, New York, 1998), Chap. 6, pp. 61–82.

17. S. Skupsky and R. S. Craxton, Phys. Plasmas **6**, 2157 (1999).

18. T. R. Boehly, R. S. Craxton, T. H. Hinterman, P. A. Jaanimagi, R. L. Keck, J. H. Kelly, T. J. Kessler, R. L. Kremens, S. A. Kumpan, S. A. Letzring, R. L. McCrory, S. F. B. Morse, W. Seka, S. Skupsky, J. M. Soures, and C. P. Verdon, in *Proceedings of the IAEA Technical Committee Meeting on Drivers for Inertial Confinement Fusion*, edited by J. Coutant (IAEA, Vienna, 1995), pp. 79–86.

19. T. J. Kessler, Y. Lin, L. S. Iwan, W. P. Castle, C. Kellogg, J. Barone, E. Kowaluk, A. W. Schmid, K. L. Marshall, D. J. Smith, A. L. Rigatti, J. Warner, and A. R. Staley, in *Second Annual International Conference on Solid State Lasers for Application to Inertial Confinement Fusion*, edited by M. L. André (SPIE, Bellingham, WA, 1997), Vol. 3047, pp. 272–281.

20. W. Seka, R. S. Craxton, R. E. Bahr, D. L. Brown, D. K. Bradley, P. A. Jaanimagi, B. Yaakobi, and R. Epstein, Phys. Fluids B **4**, 432 (1992).

21. R. S. Craxton and R. L. McCrory, J. Appl. Phys. **56**, 108 (1984).

22. P. W. McKenty, V. N. Goncharov, R. P. J. Town, S. Skupsky, R. Betti, and R. L. McCrory, Phys. Plasmas **8**, 2315 (2001).